NASA TECHNICAL MEMORANDUM

NASA TM X-3198

NASA TM X-3198

STRUCTURAL ANALYSIS OF WIND TURBINE ROTORS FOR NSF-NASA MOD-0 WIND POWER SYSTEM

David A. Spera

Lewis Research Center

Cleveland, Ohio 44135

NATIONAL AERONAUTICS AND SPACE ADMINISTRATION • WASHINGTON, D. C. • MARCH 1975

1. Report No.	2. Government Accession No.	3. Recipient's Catalog No.
NASA TM X-3198		N75-17712

4. Title and Subtitle	5. Report Date
STRUCTURAL ANALYSIS OF WIND TURBINE ROTORS FOR NSF-NASA MOD-0 WIND POWER SYSTEM	March 1975
	6. Performing Organization Code
7. Author(s)	8. Performing Organization Report No.
David A. Spera	E-8133
	10. Work Unit No.
9. Performing Organization Name and Address	778-00
Lewis Research Center National Aeronautics and Space Administration Cleveland, Ohio 44135	11. Contract or Grant No.
	13. Type of Report and Period Covered
12. Sponsoring Agency Name and Address	Technical Memorandum
National Aeronautics and Space Administration Washington, D.C. 20546	14. Sponsoring Agency Code

15. Supplementary Notes

16. Abstract

Preliminary estimates are presented of vibratory loads and stresses in hingeless and teetering rotors for the proposed 100-kW wind power system. Stresses in the shank areas of the 19-m (62.5-ft) blades are given for static, rated, and overload conditions. The teetering rotor has substantial advantages over the hingeless rotor with respect to shank stresses, fatigue life, and tower loading. A teetering rotor will probably be required in order to achieve a long service life in a large wind turbine exposed to periodic overload conditions.

17. Key Words (Suggested by Author(s))	18. Distribution Statement
Windmills; Wind-powered generators; Towers; Rotor blades; Rotary wings; Vibratory loads; Fatigue life; Wind shear	Unclassified - unlimited STAR category 39 (rev.)

19. Security Classif. (of this report)	20. Security Classif. (of this page)
Unclassified	Unclassified

* For sale by the National Technical Information Service, Springfield, Virginia 22151

STRUCTURAL ANALYSIS OF WIND TURBINE ROTORS FOR NSF-NASA MOD-0 WIND POWER SYSTEM

by David A. Spera

Lewis Research Center

SUMMARY

Preliminary estimates are presented of vibratory loads and stresses in hingeless and teetering rotors for the proposed NSF-NASA Mod-0 wind power system. The wind turbine in this system has a two-bladed rotor 38 meters (125 ft) in diameter on a 30-meter (100-ft) tower. System rated output is 100 kilowatts at a wind speed of 8 meters per second (18 mph).

Preliminary blade design utilizes a tapered tubular aluminum spar which supports nonstructural aluminum ribs and skin and is joined to the rotor hub by a steel shank tube. Stresses in the shank of the blade are calculated for static, rated, and overload operating conditions. Blade vibrations were limited to the fundamental flapping modes, which were elastic cantilever bending for hingeless rotor blades and rigid-body rotation for teetering rotor blades. The MOSTAB-C computer code was used to calculate aerodynamic and mechanical loads.

The teetering rotor has substantial advantages over the hingeless rotor with respect to shank stresses, fatigue life, and tower loading. The hingeless rotor analyzed does not appear to be structurally stable during overloads. Therefore, until adequate reliability of associated automatic controls has been established, a teetering rotor will probably be required in order to achieve a long service life in a wind turbine which operates unattended.

INTRODUCTION

Large wind turbines must be designed for structural efficiency and reliability together with minimum maintenance and weight in order to produce energy at a competitive cost. Major factors which dictate structural weight are the vibratory loads which act on the rotor and the tower. These unsteady loads may be aerodynamic, gravitational, or inertial in origin. For very large wind turbines (e.g., diameters larger than 30 m

(100 ft)), vibratory stresses caused by dynamic loads will probably be the governing design consideration (ref. 1).

This study was conducted to estimate the dynamic loads and vibratory stresses which may occur in two types of rotors for the proposed NSF-NASA Mod-0 wind power system* (ref. 2). As shown in figure 1 the wind turbine in this system will have a two-bladed rotor 38 meters (125 ft) in diameter on a tower 30 meters (100 ft) in height. The rated electrical output is to be 100 kilowatts at a wind velocity of 8 meters per second (18 mph). It will be located at the NASA Lewis Research Center Plum Brook Station near Sandusky, Ohio.

Of particular interest to the designers of the Mod-0 wind turbine are the advantages of articulating (or hinging) the rotor blades, as is commonly done in helicopters. The simplest articulation method is "teetering," in which a pair of connected blades are fastened to the rotor shaft by means of a pivot pin. This permits a teetering (or see-saw) motion of the blades parallel to the shaft, which can reduce internal bending stresses in the blades and vibratory loads on the tower. A teetering rotor was used successfully in the 100-kilowatt Hutter-Allgaier wind generator system (ref. 3). The hub of this rotor is shown schematically in figure 2.

In this study the advantages of a teetering rotor are determined quantitatively by direct comparison of vibratory loads and stresses in a teetering rotor with those in a hingeless design. Because of the preliminary nature of this investigation, stress analysis was restricted to the shank area of the blades, using elementary strength-of-materials equations. Rotor loads on the tower were also compared for the two types of construction.

A similar analysis was made by Wilcox and his coworkers together with von Karman on the 1250-kilowatt Smith-Putnam wind power system, in an effort to minimize vibratory loads on the tower (ref. 4). Only rigid-body motions of the rotor blades were considered. Each blade was individually hinged and restrained by an adjustable damper. Their analysis indicated that the undamped condition produced much smaller vibratory loads than the fully damped (hingeless) condition. This conclusion was verified by their tests on the wind turbine.

Two wind conditions were selected for estimating the effects of rotor teetering: the rated condition with a nominal wind speed of 8 meters per second (18 mph), and an overload condition with a wind speed of 27 meters per second (60 mph). In both cases the rotor speed was 4.2 radians per second (40 rpm) with the rotor axis horizontal and pointing directly into the wind. A static condition was also selected as a baseline case for comparison purposes, with zero rotor speed and a wind speed of 27 meters per second (60 mph).

---

*Cooperative project of the National Science Foundation and the National Aeronautics and Space Administration.

Certain simplifying assumptions are made in this preliminary analysis. The most important of these is that the dominant vibration mode of the rotor blades is parallel to the axis of revolution. This is the so-called "flapping" mode. Vibrations in the plane of revolution ("lead-lag" mode) and torsional vibrations are not considered. It is assumed that lead-lag and torsional vibrations are similar for both the hingeless and teetering rotors and therefore can be neglected when comparing the two rotors. For the same reason, stress concentrations and rotor-tower dynamic coupling are also neglected. Because of these assumptions, loads and stresses obtained in this study are presented as estimates for comparison purposes only. For detailed design the effects of other modes of vibration, aerodynamic instabilities, rotor-tower dynamic coupling, and stress concentrations must be considered.

The U.S. customary system of units was used in this analysis. Conversion to the International System of Units (SI) was for reporting purposes only.

SYMBOLS

A	spar cross-sectional area
a_0 to a_5, b_0 to b_3, c_0 to c_4, d_0 to d_2	polynomial series coefficients for spanwise distribution of weight, stiffness, and flapping deflection
E	modulus of elasticity
e	eccentricity
F	force
g	acceleration of gravity
I	area moment of inertia
K	kinetic energy function
ℓ	length of blade
M	bending moment
P	potential energy function
p	point on spar
q	blade weight per unit length
R	rotor axis

r	spar radial coordinate
S	spar section modulus
s	station along blade axis
T	tower axis
U	energy
V	wind velocity
W	weight
w	axial (flapping) displacement
x, y, z	Cartesian coordinates
β	flapping angle
Γ_1, Γ_2 γ_1, γ_2	dimensionless weight and stiffness functions
η	dimensionless spar radial coordinate
Θ	elevation or coning angle
ϑ	pitch angle
ξ	dimensionless axial displacement
σ	normal stress
τ	shear stress
Ψ	azimuth (constant)
ψ	azimuth (variable)
Ω	rotor rotational speed
ω	natural frequency

PRELIMINARY ROTOR DESIGN

Figure 3 shows the two rotor hub designs under consideration. In the hingeless rotor, flapping motion can occur only by elastic deformation. Bending of the blade changes the slope at its tip by an angle β, which is termed the flapping angle. The slope at the hub is unchanged from its initial value, which is defined as the blade coning angle Θ_b. In the teetering rotor the blade centerline is assumed to remain straight during flapping, with the entire blade rotating about the teetering hinge through the flapping

angle β. At the same time the opposing blade rotates through an angle $-\beta$. The first mode of flapping in this case is one of rigid-body rotation.

The preliminary external shape of the rotor blade is shown in figure 4. The blade has a total length of 19 meters (62.5 ft) and tapers from a chord of 137 centimeters 54 in.) at the hub to 46 centimeters (18 in.) at the tip. The coning angle is 0.19 radian. Cross sections are NACA airfoils of the 23 000 series with 0.2 radian of twist between hub and tip. Blade pitch is variable, to control speed.

The material for this preliminary blade is metal, although future blades may well be fabricated from nonmetallic composites. The blade structure is assumed to consist of a tapered aluminum tubular spar supporting nonstructural ribs and skin. The hub end of this spar has an outer diameter of 50.8 centimeters (20 in.) and an inner diameter of 48.3 centimeters (19 in.). A steel tube joins the spar to the hub, forming the shank of the blade. Preliminary dimensions of this tube are an outer diameter of 32.4 centimeters (12.75 in.) and an inner diameter of 27.9 centimeters (11 in.).

Preliminary estimates of the weight and stiffness distributions in the metal rotor blade are shown in figure 5. The weight of 8900 newtons (2000 lbf) per blade is the upper limit for the Mod-0 wind turbine. Lighter blades are desirable because they would lower both dynamic and static loads, with resulting benefits in system reliability and cost. Substantial reductions in weight, of the order of 50 percent, may be achieved by using composites in future blades. No balance weights are included in this weight estimate.

It is assumed that only the main spar contributes to the bending stiffness. Because this spar is a round tube, bending stiffnesses are equal in both the flapping and lead-lag directions.

LOAD AND STRESS ANALYSIS

Wind Turbine Coordinate Systems

Before proceeding with the load and stress analysis it is necessary to establish coordinate systems for the wind turbine. These are shown in figure 6. Four coordinate systems are required: tower, rotor, blade, and spar. Coordinate axes in these four systems are designated by the subscripts t, r, b, and s, respectively.

In the tower coordinate system the origin is at the intersection of the tower axis T and the rotor axis R, which establish a reference plane R-T. The x_t axis is vertically upward along the tower centerline. The y_t and z_t axes lie in a horizontal plane, with z_t along its intersection with the R-T plane and pointing away from the rotor. The wind vector is located with respect to the horizontal plane by an azimuth Ψ_w,

measured from the z_t axis, and an elevation angle Θ_w. The rotor axis is located by the elevation angle Θ_r and has an azimuth of 180^o, with respect to the z_t axis.

The origin of the rotor coordinate axis is located a distance e_r along the rotor axes from the origin of the tower axes. The axes x_r and y_r lie in the plane of revolution and rotate with the blades at an angular velocity Ω. The azimuth ψ_b locates x_r with respect to the R-T plane. The z_r axis is along the rotor axis, pointing toward the tower.

The blade axis is located with respect to the plane of revolution by the azimuth angle ψ_b and the elevation (coning) angle Θ_b. The origin of the blade system is located a distance s along the blade axis, in a direction opposite to that of x_r. The x_b axis lies along the blade axis, pointing toward the rotor axis. The y_b axis is the chord line of the airfoil section. It is located by the pitch angle ϑ with respect to the plane of revolution and points toward the leading edge of the blade. The z_b axis is usually the quarter-chord line.

The spar coordinate axes are parallel to the blade axes, with their origin displaced a distance e_s along the z_b axis toward the suction side of the airfoil. Finally, any point p on the spar for which stresses are to be calculated is located by an azimuth ψ_s.

Blade Reactions

The blade root reactions at the shaft centerline were obtained by using the MOSTAB-C computer code (ref. 5). These reactions are for one blade, either hinged or hingeless, vibrating only in the flapping mode under steady-state conditions. They consist of three forces and three moments referred to the rotor coordinate system:

$$\left.\begin{matrix} F_{x,r} \\ F_{y,r} \\ F_{z,r} \end{matrix}\right\} \text{Root forces} \qquad (1a)$$

$$\left.\begin{matrix} M_{x,r} \\ M_{y,r} \\ M_{z,r} \end{matrix}\right\} \text{Root moments} \qquad (1b)$$

These reactions must be transferred to the spar coordinate system before stresses can be calculated. The transfer equations are as follows:

$$F_{x,s} = F_{x,r} \cos \Theta_b + F_{z,r} \sin \Theta_b \tag{2a}$$

$$F_{y,s} = F_{y,r} \cos \vartheta - (F_{z,r} \cos \Theta_b - F_{x,r} \sin \Theta_b) \sin \vartheta \tag{2b}$$

$$F_{z,s} = (F_{z,r} \cos \Theta_b - F_{x,r} \sin \Theta_b) \cos \vartheta + F_{y,r} \sin \vartheta \tag{2c}$$

$$M_{x,s} = M_{x,r} \cos \Theta_b + M_{z,r} \sin \Theta_b - e_s F_{y,s} \tag{2d}$$

$$M_{y,s} = M_{y,r} \cos \vartheta - (M_{z,r} \cos \Theta_b - M_{x,r} \sin \Theta_b) \sin \vartheta + e_s F_{x,s} - s F_{z,s} \tag{2e}$$

$$M_{z,s} = (M_{z,r} \cos \Theta_b - M_{x,r} \sin \Theta_b) \cos \vartheta + M_{y,r} \sin \vartheta + s F_{y,s} \tag{2f}$$

in which

Θ_b coning angle

ϑ pitch angle

s distance from rotor axis to spar section

e_s eccentricity of spar with respect to blade axes

The coning angle Θ_b is assumed to be approximately equal to the average angular elevation of the blade from the plane of revolution (the x_r-y_r plane). Also, aerodynamic and inertia loads are assumed to be negligible within the length s.

Spar Stresses

The spar is assumed to be a hollow round cylinder with inner radius r_i and outer radius r_o. The axial normal stress σ_x at a point p on the outer surface of this cylinder (fig. 6) is

$$\sigma_x = -\frac{F_{x,s}}{A} + \frac{1}{S}(M_{z,s} \cos \psi_s - M_{y,s} \sin \psi_s) \tag{3a}$$

in which

$$\left.\begin{aligned} A &= \pi\left(r_o^2 - r_i^2\right) \quad \text{spar cross-sectional area} \\ S &= \frac{\pi}{4r_o}\left(r_o^4 - r_i^4\right) \quad \text{spar section modulus} \end{aligned}\right\} \tag{3b}$$

and ψ_s is the azimuth of point p. The shearing stress $\tau_{x,\psi}$ at point p is

$$\tau_{x,\psi} = \frac{1}{S}\left[-\frac{M_{x,s}}{2} + \frac{r_o^2 + r_o r_i + r_i^2}{r_o}\left(F_{y,s}\sin\psi - F_{z,s}\cos\psi\right)\right] \tag{4}$$

The remaining components of stress are assumed to be negligible, or

$$\sigma_\psi = \sigma_r = \tau_{x,r} = \tau_{\psi,r} = 0 \tag{5}$$

The axial and shearing stresses can be combined into principal and effective stresses as follows:

$$\sigma_1 = \frac{\sigma_x}{2} + \tau_{max} \tag{6a}$$

$$\sigma_2 = \frac{\sigma_x}{2} - \tau_{max} \tag{6b}$$

in which

$$\tau_{max} = \sqrt{\left(\frac{\sigma_x}{2}\right)^2 + \tau_{x,\psi}^2} \tag{6c}$$

and the effective stress is

$$\sigma_e = \sqrt{\sigma_x^2 + 3\tau_{x,\psi}^2} = \sqrt{\sigma_1^2 - \sigma_1\sigma_2 + \sigma_2^2} \tag{7}$$

Rotor Loads on Tower

The root reactions from two blades combine as follows to form the rotor loads on the tower, referred to the tower coordinate system (fig. 6):

$$F_{x,t} = (F_{x,2r} \cos \psi_b + F_{y,2r} \sin \psi_b) \cos \Theta_r - F_{z,2r} \sin \Theta_r \tag{8a}$$

$$F_{y,t} = F_{y,2r} \cos \psi_b - F_{x,2r} \sin \psi_b \tag{8b}$$

$$F_{z,t} = F_{z,2r} \cos \Theta_r + (F_{x,2r} \cos \psi_b + F_{y,2r} \sin \psi_b) \sin \Theta_r \tag{8c}$$

$$M_{x,t} = (M_{x,2r} \cos \psi_b + M_{y,2r} \sin \psi_b) \cos \Theta_r - M_{z,2r} \sin \Theta_r + e_r F_{y,t} \cos \Theta_r \tag{8d}$$

$$M_{y,t} = M_{y,2r} \cos \psi_b - M_{x,2r} \sin \psi_b - e_r F_{x,t} \cos \Theta_r - M'_{y,t} \tag{8e}$$

$$M_{z,t} = M_{z,2r} \cos \Theta_r + e_r F_{y,t} \sin \Theta_r \tag{8f}$$

in which

ψ_b azimuth of first blade

Θ_r elevation angle of rotor axis

e_r distance from origin of tower coordinates to origin of rotor coordinates

$$F_{x,2r} = F_{x,r}\Big|_{\psi_b} - F_{x,r}\Big|_{\psi_b+180^\circ} \tag{9a}$$

$$F_{y,2r} = F_{y,r}\Big|_{\psi_b} - F_{y,r}\Big|_{\psi_b+180^\circ} \tag{9b}$$

$$F_{z,2r} = F_{z,r}\Big|_{\psi_b} + F_{z,r}\Big|_{\psi_b+180^\circ} \tag{9c}$$

$$M_{x,2r} = M_{x,r}\Big|_{\psi_b} - M_{x,r}\Big|_{\psi_b+180^o} \tag{9d}$$

$$M_{y,2r} = M_{y,r}\Big|_{\psi_b} - M_{y,r}\Big|_{\psi_b+180^o} \tag{9e}$$

$$M_{z,2r} = M_{z,r}\Big|_{\psi_b} + M_{z,r}\Big|_{\psi_b+180^o} \tag{9f}$$

and $M'_{y,t}$ is the moment of the superstructure without the blades. If we assume that the superstructure with blades is statically balanced on the tower,

$$M'_{y,t} = 2W_b(e_r + e_b)\cos\Theta_r \tag{9g}$$

in which e_b is the axial distance along the rotor axis from the origin of the rotor coordinates to the centroid of the blades, and W_b is the weight of one blade.

The components of the rotor loads on the tower can be combined into a resultant force and a resultant moment, as follows:

$$F_t = \sqrt{F_{x,t}^2 + F_{y,t}^2 + F_{z,t}^2} \tag{10a}$$

$$M_t = \sqrt{M_{x,t}^2 + M_{y,t}^2 + M_{z,t}^2} \tag{10b}$$

WIND LOADS

Operating Conditions

Loads and stresses were calculated for the teetering and hingeless rotors under three operating conditions: static, rated, and overload. The static condition was used as a reasonably severe baseline against which to compare the two dynamic conditions. In the static case the wind speed is 27 meters per second (60 mph) and the blades are stopped in the horizontal position with their chords perpendicular to the wind for maximum aerodynamic loading.

In the rated operating condition the wind speed is 8 meters per second (18 mph), and rotor speed is 4.2 radians per second (40 rpm). Blade pitch is -0.10 radian at the hub. The blades produce 150 kilowatts of mechanical power (200 hp) at this pitch. This provides 50 kilowatts for losses and an output of 100 kilowatts of electrical power.

In the overload condition the wind speed is 27 meters per second (60 mph), rotor speed remains at 4.2 radians per second (40 rpm), and approximately 75 kilowatts (100 hp) are produced with -0.30-radian pitch. Under these conditions the blades are on the verge of a flapping instability which would cause large flapping angles and impact of the blade on the hub stops and possibly the tower. Flapping angle amplitude for the teetering blade at the overload condition is about $\pm 10^{\circ}$. This value would increase rapidly with a slight increase in wind velocity or decrease in pitch angle. Thus, the overload condition represents an extremely severe operating condition which the turbine would experience for only a very short time, if ever.

Wind Shear

The earth's roughness produces a boundary layer which creates a gradient in wind velocity with altitude. This gradient is usually expressed in terms of the altitude to a fractional power. However, in the MOSTAB-C computer code the simplifying assumption is made that wind velocity V varies linearly with altitude, within the limits of the rotor, so that

$$V = V_0 \left(1 + \delta \frac{s}{l} \sin \psi_b\right) \tag{10a}$$

in which

V_0 nominal wind velocity at elevation of rotor axis

δ constant which depends on ratio l/h_t

l blade length

h_t tower height

s station along blade axis from rotor axis

ψ_b blade azimuth

Defining wind shear ΔV as the difference between the maximum and minimum wind velocities, equation (10a) gives

$$\Delta V = \delta V_0 \tag{10b}$$

It can be seen from equation (10a) that wind shear produces a periodic wind load with a frequency of once per revolution. This is the only frequency of blade vibration which can be excited by the wind shear.

In this preliminary analysis the constant δ was assumed to be 0.15 for a ratio of blade length to tower height of 0.62. This results in a wind shear of 1.2 meters per second (2.7 mph) at the design operating condition. This is probably not a conservative amount of wind shear and δ should be increased in future computations to about 0.20 for high wind velocities and 0.30 for low velocities.

Tower Wake

An important source of periodic wind load is the aerodynamic interference created by the tower, which is upwind of the rotor. This is referred to as the tower wake effect. The magnitude of this periodic load is determined by the projected area of the tower structural elements, their average drag coefficient, and the sector of the rotor area affected by the wake. The truss tower shown in figure 1 was assumed to have a projected area of 37 square meters (400 sq ft) when oriented diagonally to the wind. A conservative value of 2.0 was used for its average drag coefficient. Blades were assumed to be in the tower wake at azimuths from 345° to 15°.

Although the tower wake has a fundamental frequency of once per revolution, it is a pulse load which can contain harmonics at many frequencies. Therefore, the tower wake is a potential excitation source for vibrations at any integer multiple of the rotational speed.

RESULTS AND DISCUSSION

Blade Natural Frequencies

Vibrations of the rotor blades in service are based on their natural frequencies. In this analysis, only the first, or fundamental, mode of flapping vibration is considered; so only this natural frequency is required. Equations for calculating the flapping natural frequency of a rotating blade are given in the appendix. For the hingeless blade the assumed mode shape is the static deflection curve. For the teetering blade the assumed mode shape is a straight line.

The variation in natural frequency with rotor speed is presented in figure 7. Both quantities are normalized with respect to the design speed of 4.2 radians per second (40 rpm). The hingeless blade has a normalized natural frequency which varies from

2.65 to 2.88 as the rotor speed increases from zero to the design speed. Plotted in figure 7 are integer multiples of the normalized rotor speed, which indicate potential excitation frequencies. The line for three cycles per revolution (3P) crosses the natural frequency line for the hingeless blade at slightly under the design speed. This indicates that three flapping vibrations per revolution might be expected at the design speed. As shown in a later section, these vibrations do occur and are excited by the tower wake.

The rigid-body motion of the teetering blade has a normalized natural frequency of 0.96, calculated by using equation (A10). Thus, the teetering blade experiences one cycle of vibration per revolution, which is excited by the wind shear, the tower wake, and gravity. The lead-lag frequency ratio for both the hingeless and teetering blades is 2.65 and does not change with rotor speed.

These values of normalized natural frequency indicate that the metal blades are quite stiff and probably not prone to high vibration stresses under normal operating conditions. This can best be shown by comparing their frequencies to those of other rotor systems, as is done in figure 8.

In figure 8, typical lead-lag and flapping frequency ratios are given for conventional propellers and several types of helicopter rotors. These data and the estimates for wind turbines were taken from reference 1. It can be seen that the Mod-0 blades are at least one integer multiple higher in normalized frequency than equivalent helicopter rotors or propellers. This substantially decreases the chances of exciting resonances or instabilities during service.

Coning Angle

The coning angle Θ_b was determined to be 11° (0.19 rad) by the procedure illustrated in figure 9. This figure shows the flapping angle β for a single hinged blade without initial coning, as a function of the blade azimuth ψ_b. The variation is sinusoidal, with a mean value of about 11° and an amplitude of 1.5°. The mean value is determined by the direction of the resultant of the centrifugal and aerodynamic loads at the hinge line at the design wind condition. If this mean value is used as the coning angle for a two-bladed teetering rotor, root bending moments will remain essentially zero. One blade can experience positive flapping while the other, 180° out of phase, experiences an equal amount of negative flapping.

The same coning angle was used for both the hingeless and teetering rotors at both the rated and overload wind conditions. However, 11° is not necessarily the optimum coning angle for operation over a range of wind conditions. Because the wind speed will usually be between 4 and 8 meters per second (9 and 18 mph) during operation, a compromise coning angle of 7° will probably be used for the first Mod-0 blades.

The flapping amplitude of 1.5° is composed of the following components: gravity (because of coning), 0.8°; tower wake, 0.2°; and wind shear, 0.5°. Each of these components varies in an approximately linear fashion with respect to its load parameter. For example, doubling the wind shear constant δ from 0.15 to 0.30 increases the flapping amplitude by 0.5°. The sinusoidal variation in flapping angle is equivalent to a 1.5° rotation of the plane of revolution about a vertical axis through the hub. Thus, the rotor reacts like a gyroscope to the moments caused by gravity, tower wake, and wind shear. These moments are all about a horizontal axis in the plane of revolution. However, they cause a rotation about a vertical axis, analogous to gyroscope precession.

Blade Root Reactions

Figures 10 to 12 present the force and moment reactions at the root of one blade as a function of blade azimuth angle. These reactions are all referred to the rotor coordinate system and are for the rated operating condition. In these and the following figures, values for the teetering rotor are shown by dashed lines and those for the hingeless rotor by solid lines.

As shown in figure 10 both the radial and tangential root forces for the teetering rotor are approximately equal to those for the hingeless rotor. The mean value of the tangential force $F_{y,r}$ is the aerodynamic lift on the blade in the direction of rotation. Superimposed on this is a sinusoidal gravity force whose amplitude is the blade weight. The blade weight is five times the lift force, which indicates that gravity rather than wind is the dominant source of load at the rated condition. The mean value of the radial force $F_{x,r}$ is the centrifugal loading on the blade root. Again, a sinusoidal gravity force is superimposed on it, 90° out of phase with that in the tangential direction.

Figure 11 shows torque and twist moments at the blade root, which are also the same for both the teetering and hingeless rotors. The maximum weight torque occurs when the blade is horizontal at azimuths of 90° and 270°. This weight torque is three times the "working" torque required to produce the rated power of 75 kilowatts per blade. This emphasizes the dominant role of gravity at the design operating condition. The blade weight appears to be disproportionately large compared to aerodynamic forces. Bending loads and stresses are a maximum at an azimuth of 270°, where the weight and working torques are in the same direction. This is the critical reaction for stress analysis at the rated operating condition. The twisting moment $M_{x,r}$ is primarily gravitational, resulting from the coning of the blade. Centrifugal untwisting is neglected in this analysis.

Figure 12 shows the two root reactions which are different for the teetering and hingeless rotors. These are the axial force and the flapping moment, both of which are

affected by flapping motions of the blade. In figure 12(a) the flapping moment $M_{y,r}$ for the teetering rotor is approximately zero because of the flapping hinge and the chosen coning angle. However, the hingeless blade experiences a significant oscillatory flapping moment with three peaks per revolution. This is the 3P elastic vibration indicated by the natural frequency chart (fig. 7).

The maximum flapping moment in the hingeless blade occurs at an azimuth of 30°. This indicates that maximum deflections will lag maximum loads by a phase angle of about 30° in this blade. The maximum flapping moment is composed of gravity, wind shear, and tower wake components in the following proportions: gravity (1P), 25 percent; wind shear (1P), 20 percent; and tower wake (3P), 55 percent. The tower wake pulse apparently contains a significantly large third harmonic, which excites the hingeless blade at its natural frequency.

According to equation (9e) the resultant load on the tower from two blades is the difference of flapping moments 180° out of phase in azimuth. As shown by points 1 and 2 in figure 12(a) the maximum and minimum flapping moments are also 180° out of phase in the hingeless rotor. Thus, the tower will be subjected to a peak bending moment which is the sum of the two most severe flapping moments for one blade.

In figure 12(b) the axial force on the hingeless rotor blade also shows a 3P vibration about the average aerodynamic drag force. On the other hand the teetering blade exhibits a smooth sinusoidal variation in axial force at its root, which is caused by inertia forces accompanying its rigid-body vibration.

In summary, four of the six reactions at the blade root are the same for both the teetering and hingeless rotors at the design operating condition. Included in these is the critical reaction for stress analysis, which is the torque moment. Gravity loads are dominant over aerodynamic and inertia loads. However, the hingeless blade experiences a 3P elastic flapping vibration, which could result in tower excitation or high vibratory blade stresses at higher wind speeds.

Blade Shank Stresses

The axial stress σ_x is the dominant stress component in the effective stress (eq. (7)). The shear stress $\tau_{x,\psi}$ is small in the blade shank area. Figure 13 shows the critical axial stress cycles at two locations in the shank of the blade under the design operating conditions. These stress cycles would be the determining factor in the fatigue life of the blade root and probably of the entire blade. The absolute values of stress shown here are not significant except for the fact that they are low enough to indicate that the preliminary blade design is feasible for both types of rotors. These stresses do not include a stress concentration factor.

Point A is 1.0 meter from the rotor axis on the trailing edge of the steel tube which joins the airfoil section of the blade to the hub. Preliminary dimensions of this tube are an outer diameter of 32.4 centimeters (12.75 in.) and an inner diameter of 27.9 centimeters (11.0 in.).

Point B is 1.5 meters from the rotor axis on the trailing edge of the tapered aluminum spar where it joins the steel shank tube. Preliminary dimensions of the spar at this radial station are an outer diameter of 50.8 centimeters (20.0 in.) and an inner diameter of 48.3 centimeters (19.0 in.).

As shown in figure 13, critical stresses are approximately equal for the teetering and hingeless rotors. The reason for this equality is that the critical root reaction at the design condition is the torque moment shown in figure 10. This moment is the same for both rotors because it is determined by the rated power and the blade weight.

Critical stress cycles for the static, rated, and overload conditions are summarized in table I. These stresses are expressed in terms of baseline stresses σ_A and σ_B obtained for the static condition. In this condition the blades are stationary in the horizontal position with their chord planes facing the wind. The weight of the blade and the aerodynamic drag produce the baseline stresses in the table.

As was shown in figure 13 the critical stress cycles for the teetering and hingeless rotors are approximately equal at the rated condition. However, at the severe overload condition the stresses in the teetering blade are only about one-half those in the hingeless blade. Moreover, the cyclic frequency for the teetering blade is only one-third that for the hingeless blade.

During overload conditions the stress and frequency advantages of the teetering blade over the hingeless blade combine to greatly reduce its relative rate of fatigue damage. As a preliminary estimate the damage rate in the teetering blade during overload would probably be less than one-twentieth that in the hingeless blade. In other words, if the wind turbine were to approach an instability condition in which the blades begin moderate to large flapping vibrations, fatigue damage to a teetering blade would be minor compared to that in a hingeless blade for equal periods of time.

An estimate of the relative importance of fatigue damage at the rated condition to that at overload can also be made from the data in table I. The overload stresses are considerably larger than the rated stresses for both types of rotors. This means that the blades must be designed for infinite life at the rated condition in order to have a reasonable cumulative fatigue life. Thus, the overall fatigue life of the rotor would not be determined by the blade stresses at the rated condition but by the stresses during gusts, control malfunctions, very high winds, and other abnormal operating conditions. On this basis, the life of the teetering rotor would be substantially longer than that of the hingeless rotor. A spectrum of loads from rated to overload is required for a quantitative estimate of the fatigue life advantage of the teetering rotor. Qualitatively, it is probably a factor of at least 5 to 1.

Rotor Loads on Tower

In figures 14 and 15 the loads exerted on the tower by the teetering and hingeless rotors are compared for the design condition. These loads are referred to the tower coordinate system, which is nonrotating (fig. 8). As shown in figure 14 the average forces on the tower are similar for the two rotors. However, the vibratory components of these forces are somewhat larger for the teetering rotor. This is particularly true of the side force $F_{y,t}$.

Moment loads are compared in figure 15. The shaft torque $M_{z,t}$ is identical for both rotors. As shown in the figure this torque experiences a drop in magnitude of about 20 percent each time a blade passes through the tower wake at azimuth angles of 0° and 180°. Twisting moments on the tower $M_{x,t}$ are somewhat larger in amplitude and twice as frequent for the hingeless rotor. The pitching moments on the tower $M_{y,t}$ are considerably different for the two types of rotors. At an azimuth of about 30° the hingeless rotor will exert a large pitching moment. This moment results from the two blade reactions shown in figure 12 as points 1 and 2. This moment peak is the critical rotor load on the tower.

For comparison purposes, the maximum values of the resultant force load and the resultant moment load were calculated by means of equations (10). These are summarized in table II for the three operating conditions: static, rated, and overload.

The resultant static force $F_{t,s}$ is a maximum when the stationary blades are horizontal and the chord planes are perpendicular to the wind. The maximum resultant static moment $M_{t,s}$ occurs with the blades vertical. The lower blade is assumed to be completely shielded from the wind by the tower.

At the rated wind condition the maximum force load is the same for both rotors and is about the same as the static load at the higher wind speed. Vibratory components are small and are neglected. Rated moment loads are one-third to one-half the static values for teetering and hingeless rotors, respectively.

The overload condition produces a substantial increase in tower loads for both rotors. Most significant is the maximum resultant moment load of 4.80 $M_{t,s}$ from the hingeless rotor. Under the same condition the teetering rotor exerts only one-fourth the moment on the tower.

Thus, as for the blade stresses. there is little difference between the two rotors as measured by their loads on the tower at the rated condition. However, at the overload condition, loads from a teetering rotor will be much less severe than those from a hingeless rotor.

CONCLUSIONS

Estimates were made of the vibratory loads and stresses in two types of rotors for the NSF-NASA Mod-0 wind turbine. Both hingeless and teetering rotors were analyzed under static, rated, and overload conditions. Blade vibrations were limited to the flapping mode. The following major results and conclusions were obtained:

1. A teetering rotor will probably be required in order to achieve a long service life in a wind turbine which operates unattended and is exposed to periodic overload conditions. This type of rotor has substantial advantages over a hingeless rotor with respect to shank stresses, fatigue life, and tower loading.

2. The hingeless rotor analyzed does not appear to be structurally stable during overloads which could result from high winds, severe gusts, or control malfunctions. Therefore, unattended operation of a large wind turbine with a hingeless rotor is not recommended until high reliability of associated automatic controls has been established.

3. If operations do not exceed rated conditions in severity, stresses and tower loads are about the same for both the teetering and hingeless motors analyzed in this study.

4. For a spectrum of operation between rated and overload the teetering rotor will probably have at least five times more fatigue life than the hingeless rotor.

5. For equal structural stability the tower for a hingeless rotor would have to be heavier and stiffer than that for a teetering rotor.

6. The Mod-0 rotor, either hingeless or teetering, will probably be substantially less susceptible to dynamic instability than helicopter rotors or propellers.

7. The main source of loads and stresses in both rotors is the blade weight, which is disproportionately large compared to aerodynamic forces. Efforts should be made to substantially reduce the weight of the blades, possibly by using nonmetallic composite materials.

Loads and stresses obtained in this study are presented as estimates for comparison purposes only. For detailed design the effects of other modes of vibration, aerodynamic instabilities, rotor-tower dynamic coupling, and stress concentrations must be considered.

Lewis Research Center,
National Aeronautics and Space Administration,
Cleveland, Ohio, December 4, 1974,
778-00.

APPENDIX - EQUATIONS FOR NATURAL FREQUENCY OF BLADES IN FLAPPING MODE

The derivation of the following equations follows the general procedures of references 6 and 7, with the effect of coning angle added. If we assume that the vibrating blade does not dissipate energy, its maximum potential energy equals its maximum kinetic energy, or

$$U_{p,\max} = U_{k,\max} \tag{A1}$$

in which p and k denote potential and kinetic energies, respectively. The maximum potential energy of flapping vibrations is as follows, for a blade with its root at the shaft centerline:

$$U_{p,\max} = \int_0^{l} EI_{yy}\left(\frac{d^2w}{dx^2}\right)^2 dx + \frac{\Omega^2}{2g}\cos^2\Theta_b\left[\int_0^{l} qx\int_0^{x}\left(\frac{dw}{dx}\right)^2 dx\,dx + W_t l\int_0^{l}\left(\frac{dw}{dx}\right)^2 dx\right] - \frac{\Omega^2}{2g}\sin^2\Theta_b\left[\int_0^{l} qw^2\,dx + W_t w_t^2\right] \tag{A2}$$

All coordinates are in the blade system, and

l length of blade

E modulus of elasticity

I_{yy} moment of inertia of a cross section about its y (lead-lag) axis

x axial coordinate

w maximum flapping displacement

Ω rotational speed

Θ_b coning angle

q weight per unit length

W_t concentrated weight at tip

w_t maximum tip displacement

If we assume the motion to be simple harmonic, the maximum kinetic energy of the blade is

$$U_{k,\max} = \frac{\omega_w^2}{2g}\left[\int_0^l qw^2\,dx + W_t w_t^2\right] \tag{A3}$$

in which ω_w is the unknown natural flapping frequency. The following dimensionless ratios are now defined:

$$\eta = x/l \tag{A4a}$$

$$\xi = w/l \tag{A4b}$$

$$\gamma_1 = EI_{yy}/W_b l^2 \tag{A4c}$$

$$\gamma_2 = ql/W_b \tag{A4d}$$

$$\Gamma_1 = \Omega^2 l/g \tag{A4e}$$

$$\Gamma_2 = W_t/W_b \tag{A4f}$$

in which W_b is the total weight of one blade. Introducing equations (A4) into (A2) and (A3) then gives the potential energy equation

$$U_{p,\max} = \frac{W_b l}{2} P \tag{A5a}$$

in which

$$P = \int_0^1 \left[\gamma_1(\xi'')^2 + \Gamma_1\left\{\gamma_2\left[\eta\cos^2\Theta_b\int_0^\eta(\xi')^2\,d\eta - \xi^2\sin^2\Theta_b\right] + \Gamma_2(\xi')^2\cos^2\Theta_b\right\}\right]d\eta$$

$$- \Gamma_1\Gamma_2\xi_t^2\sin^2\Theta_b \tag{A5b}$$

The kinetic energy equation becomes

$$E_{k,\max} = \omega_w^2 \frac{W_b l^2}{2g} K \tag{A6a}$$

in which

$$K = \int_0^1 \gamma_2 \xi^2 \, d\eta + \Gamma_2 \xi_t^2 \tag{A6b}$$

(Primes denote differentiation with respect to η.) Combining equations (A1), (A4a), and (A5a) yields the natural flapping frequency of the rotor blade as

$$\omega_w = \sqrt{\frac{g}{l} \frac{P}{K}} \tag{A7}$$

Hinged Rotor Blade

The first flapping mode of a hinged blade is one of rigid-body rotation. This is also the case for a teetering rotor, providing that the proper coning angle is selected to make the average flapping angle equal to zero. The mode shape and its derivatives then become

$$\left.\begin{aligned} \xi &= \beta\eta \\ \xi' &= \beta \\ \xi'' &= 0 \end{aligned}\right\} \tag{A8}$$

in which β is the flapping angle.

Combining equations (A5b), (A6b), and (A8) gives

$$P = \beta^2 \Gamma_1 \cos 2\Theta_b \left(\int_0^1 \gamma_2 \eta^2 \, d\eta + \Gamma_2 \right) \tag{A9a}$$

$$K = \beta^2 \left(\int_0^1 \gamma_2 \eta^2 \, d\eta + \Gamma_2 \right) \tag{A9b}$$

Substituting equations (A9) into (A7) then gives the natural flapping frequency for the hinged blade:

$$\omega_w = \sqrt{\frac{g}{l}\Gamma_1 \cos 2\Theta_b}$$

or

$$\omega_w = \Omega\sqrt{\cos 2\Theta_b} \tag{A10}$$

An equation similar to (A10) is given in reference 4.

Hingeless Rotor Blade

The first flapping mode shape of the hingeless blade can be approximated by its static deflection curve. By Rayleigh's principle, this approximation will lead to a calculated natural frequency which is slightly higher than the actual frequency. Polynomial series can be used to express the static deflection curve and its derivatives in terms of the distribution of stiffness and weight along the blade as follows:

$$\left.\begin{aligned} \xi &= a_0 + a_1\eta + a_2\eta^2 + a_3\eta^3 + a_4\eta^4 + a_5\eta^5 \\ \xi' &= a_1 + 2a_2\eta + 3a_3\eta^2 + 4a_4\eta^3 + 5a_5\eta^4 \\ \xi'' &= 2a_2 + 6a_3\eta + 12a_4\eta^2 + 20a_5\eta^4 \end{aligned}\right\} \tag{A11}$$

For a hingeless blade with zero deflection and rotation at the shaft centerline, the polynomial coefficients are as follows:

$$\left.\begin{aligned} a_0 &= a_1 = 0 \\ a_2 &= \frac{c_0}{2b_0} \\ a_3 &= \frac{1}{6b_0}(c_1 - 2a_2b_1) \\ a_4 &= \frac{1}{12b_0}(c_2 - 2a_2b_2 - 6a_3b_1) \\ a_5 &= \frac{1}{20b_0}(c_3 - 2a_2b_3 - 6a_3b_2 - 12a_4b_1) \end{aligned}\right\} \quad \text{(A12)}$$

in which b_0 to b_3 are curve-fit constants for the dimensionless stiffness distribution as follows:

$$\frac{EI_{yy}}{W_b l^2} = \gamma_1 = b_0 + b_1\eta + b_2\eta^2 + b_3\eta^3 \quad \text{(A13)}$$

and

$$\left.\begin{aligned} c_1 &= 1 \\ c_2 &= -\frac{d_0}{2} \\ c_3 &= -\frac{d_1}{6} \\ c_4 &= -\frac{d_2}{12} \\ c_0 &= -(c_1 + c_2 + c_3 + c_4) \end{aligned}\right\} \quad \text{(A14)}$$

The constants d_0, d_1, and d_2 are curve-fit constants for the dimensionless weight distribution, as follows:

$$\frac{q\ell}{W_b} = \gamma_2 = d_0 + d_1\eta + d_2\eta^2 \qquad \text{(A15)}$$

The natural frequency of the hingeless blade is then obtained by substituting equations (A11) to (A15) into (A5b) and (A6b).

REFERENCES

1. Ormiston, Robert A.: Rotor Dynamic Considerations for Large Wind Power Generator Systems. Wind Energy Conversion Systems, J. M. Savino, ed., NASA TM X-69786, 1973, pp. 80-88.

2. Puthoff, R. L.; and Sirocky, P. J.: Preliminary Design of a 100 kW Wind Turbine Generator. Presented at Intern. Solar Energy Soc., Ft. Collins, Colo., Aug. 21-23, 1974.

3. Hutter, U.: Operating Experience Obtained with a 100 kW Wind Power Plant. NASA TT-F-15068, 1973.

4. Putnam, Palmer C.: Power from the Wind. D. Van Nostrand Co., Inc., 1948, pp. 157-169.

5. Hoffman, John A.: Users Manual for MOSTAB-C. Rept. 4343-1, Mechanics Research, Inc., 1970.

6. Jacobsen, Lydik S.; and Ayre, Robert S.: Engineering Vibrations, with Applications to Structures and Machinery. McGraw-Hill, 1958, pp. 66-102.

7. Timoshenko, Stephen: Vibration Problems in Engineering. D. Van Nostrand Co., Inc., 1937, pp. 376-388.

TABLE I. - SUMMARY OF BLADE ROOT STRESSES

[Stress concentration factor, 1.00.]

Radial station		Operating condition	Wind speed		Axial stress cycle and frequency[a]	
m	ft		m/sec	mph	Teetering rotor	Hingeless rotor
[b]1.0	3.3	Static	27	60	1.00 σ_A	1.00 σ_A
		Rated	8	18	(0.20±0.42) σ_A; 0.67 Hz	(0.20±0.42) σ_A; 0.67 Hz
		Overload	27	60	(0.11±1.30) σ_A; 0.67 Hz	(0.16±2.24) σ_A; 2.0 Hz
[c]1.5	5.0	Static	27	60	1.00 σ_B	1.00 σ_B
		Rated	8	18	(0.25±0.41) σ_B; 0.67 Hz	(0.25±0.41) σ_B; 0.67 Hz
		Overload	27	60	(0.15±1.32) σ_B; 0.67 Hz	(0.25±2.32) σ_B; 2.0 Hz

[a] σ_A = 8600 N/cm^2 (12 500 lbf/in.^{2}); σ_B = 4900 N/cm^2 (7100 lbf/in.^{2}).
[b] Point A, where steel shank tube joins hub.
[c] Point B, where tapered aluminum spar joins steel shank tube.

TABLE II. - SUMMARY OF ROTOR LOADS ON TOWER

Type of load	Operating condition	Wind speed		Maximum resultant load and critical component frequency[a]	
		m/sec	mph	Teetering rotor	Hingeless rotor
Force	Static	27	60	1.00 $F_{t,s}$	1.00 $F_{t,s}$
	Rated	8	18	0.99 $F_{t,s}$	0.99 $F_{t,s}$
	Overload	27	60	1.48 $F_{t,s}$; 1.34 Hz	1.59 $F_{t,s}$; 2.67 Hz
Moment	Static	27	60	1.00 $M_{t,s}$	1.00 $M_{t,s}$
	Rated	8	18	0.35 $M_{t,s}$; 1.34 Hz	0.48 $M_{t,s}$; 1.34 Hz
	Overload	27	60	1.15 $M_{t,s}$; 1.34 Hz	4.80 $M_{t,s}$; 2.67 Hz

[a] $F_{t,s}$ = 38 200 N (8600 lbf); $M_{t,s}$ = 132 000 N-m (97 500 ft-lbf).

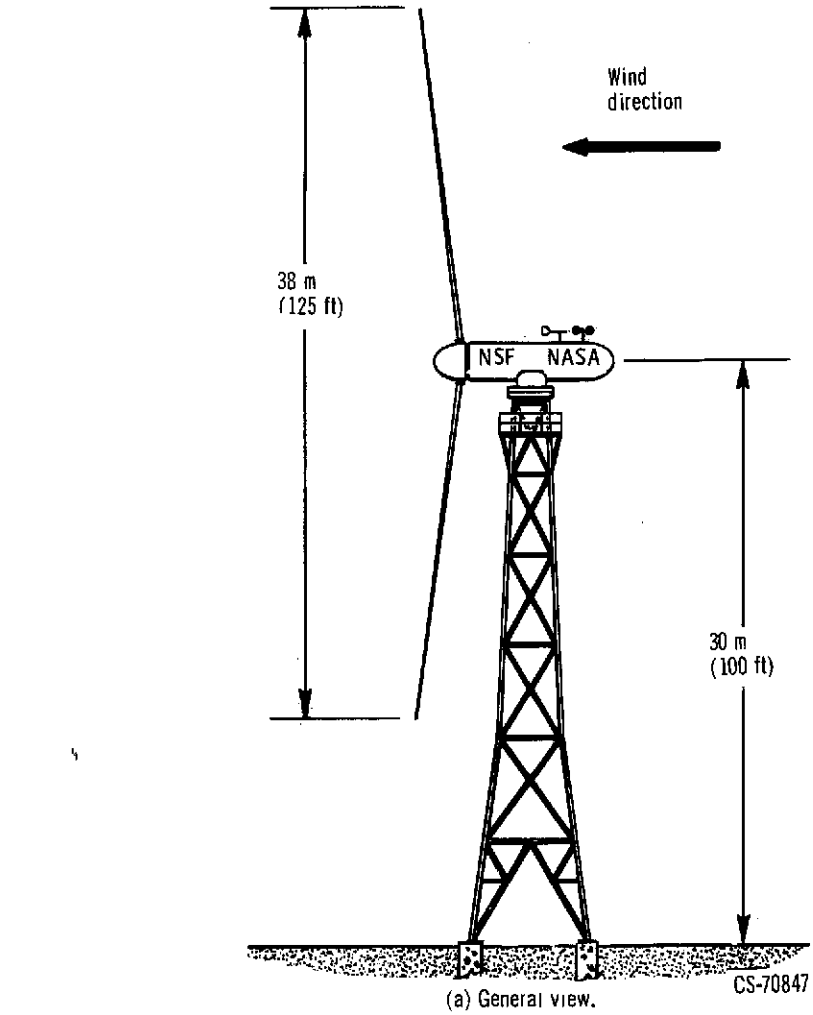

(a) General view.

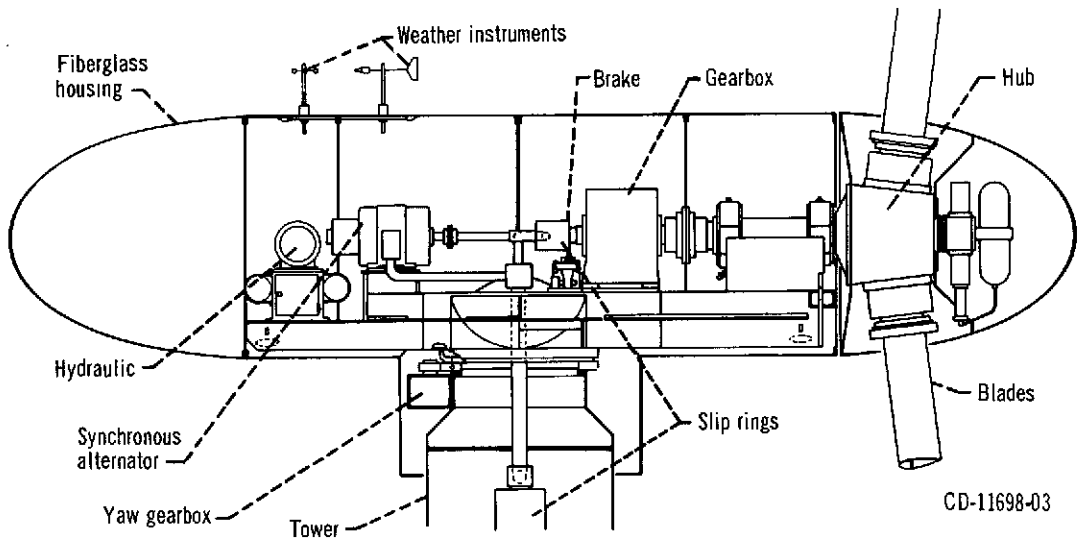

(b) Superstructure and equipment.

Figure 1. - NSF-NASA MOD-0 wind power system. Rated power output, 100 kilowatts; rated wind speed, 8 meters per second (18 mph).

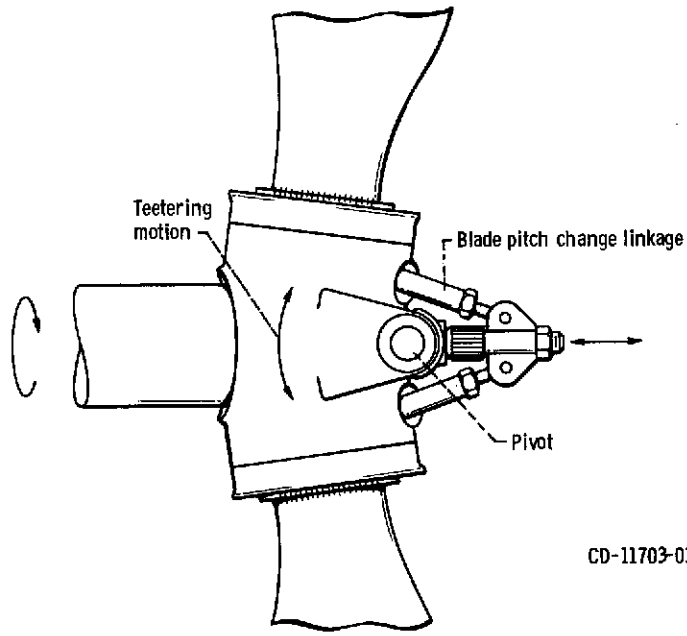

Figure 2. - Diagram of hub of teetering rotor used in 100-kilowatt Hutter-Allgaier wind power system.

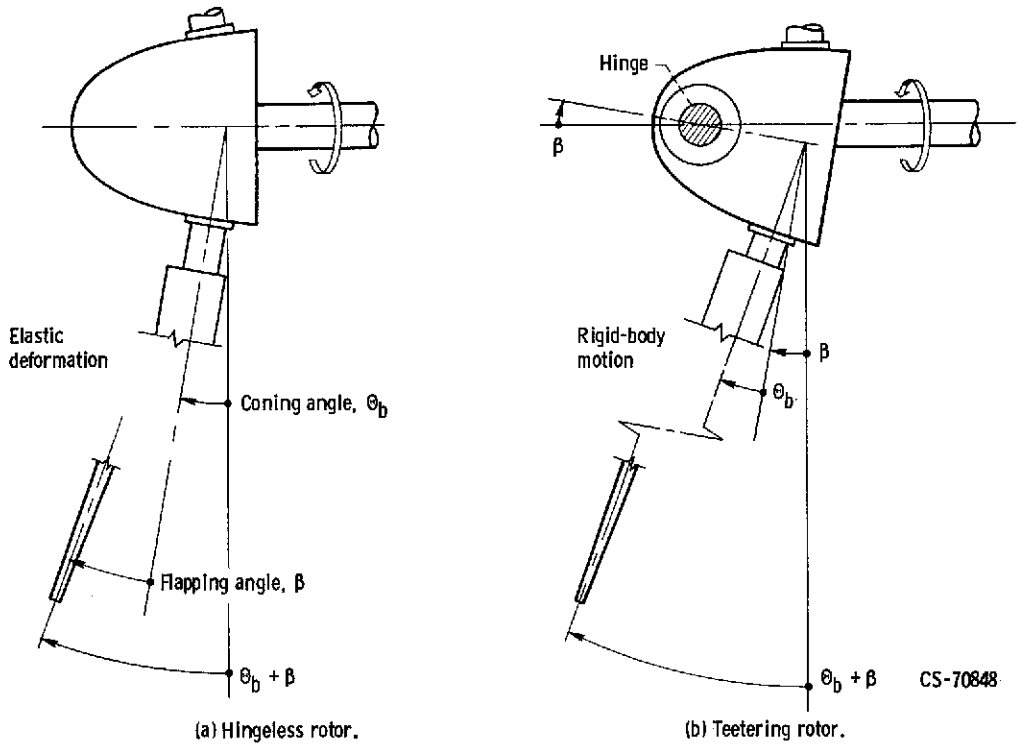

Figure 3. - Schematic illustrations of hingeless and teetering wind turbine rotors.

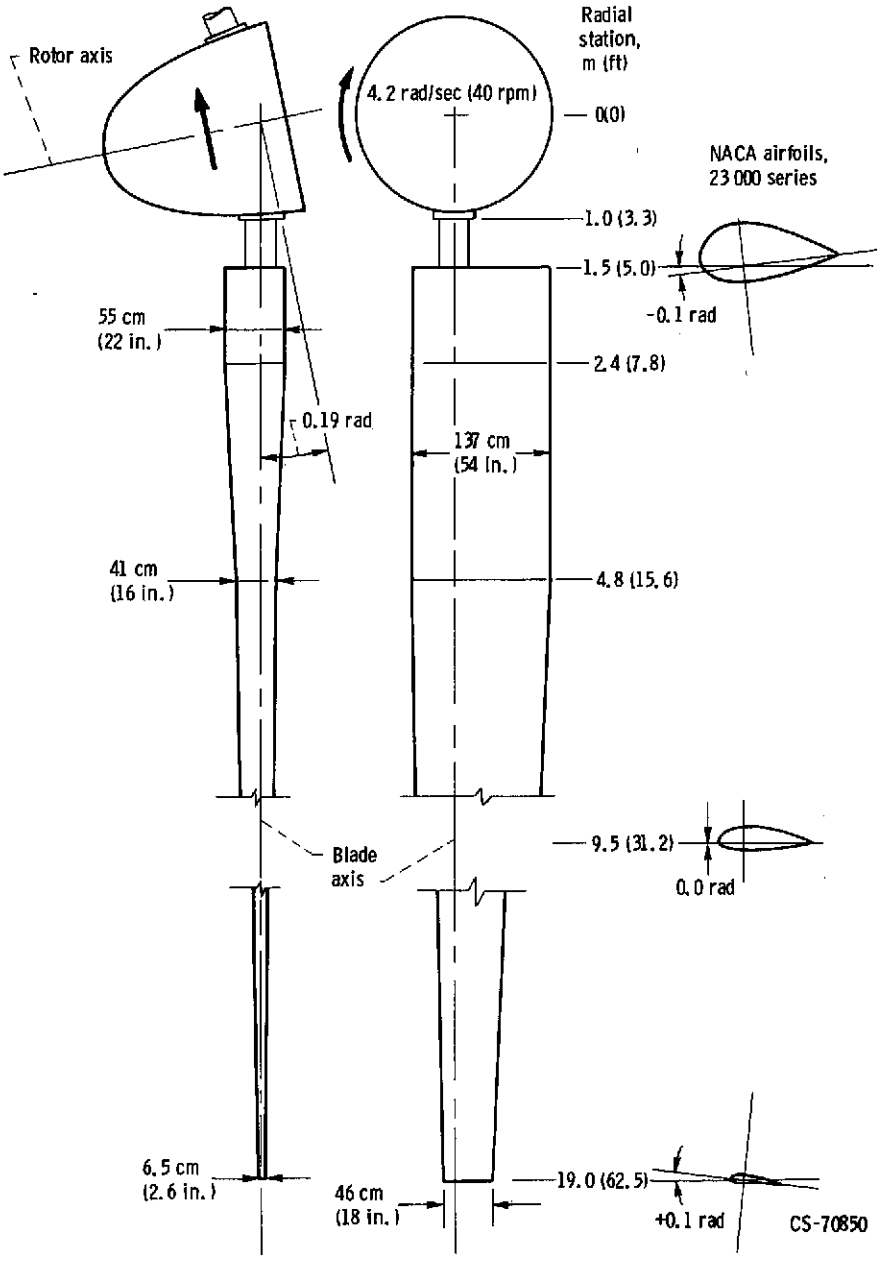

Figure 4. - Preliminary blade shape for NSF-NASA MOD-0 wind turbine.

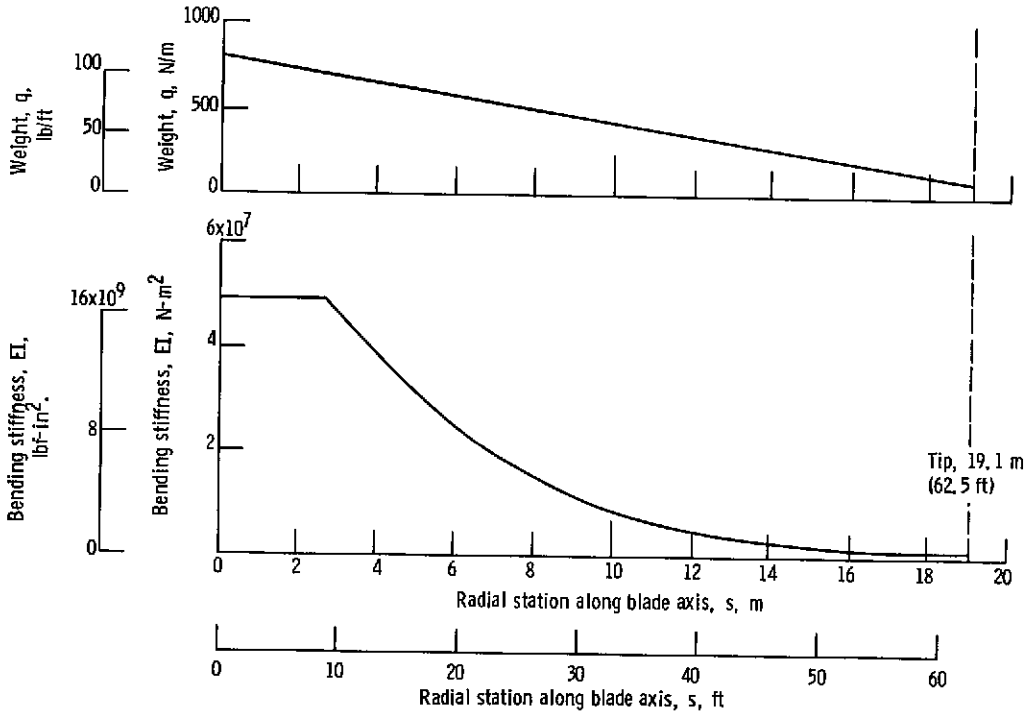

Figure 5. - Distributions of weight and stiffness of metal blade (preliminary estimates). Total weight; 8900 N (2000 lbf).

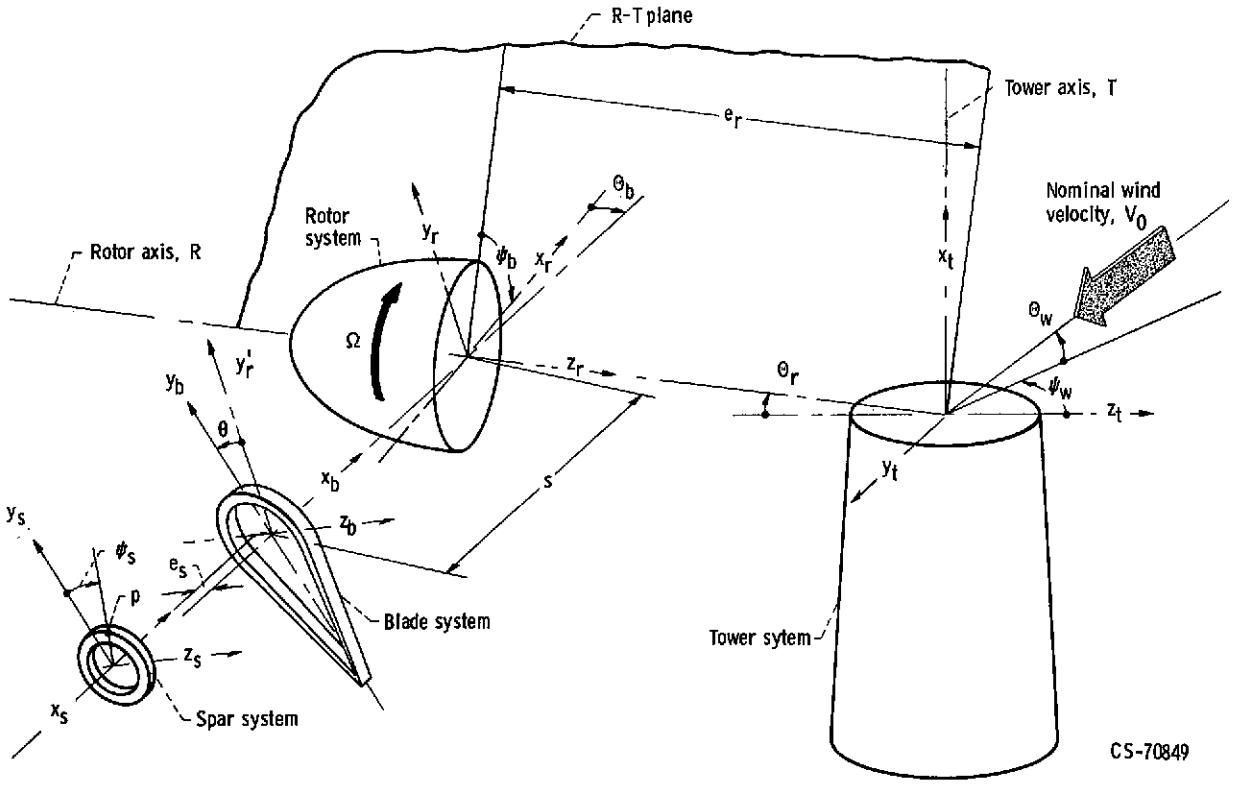

Figure 6. - Wind turbine coordinate systems.

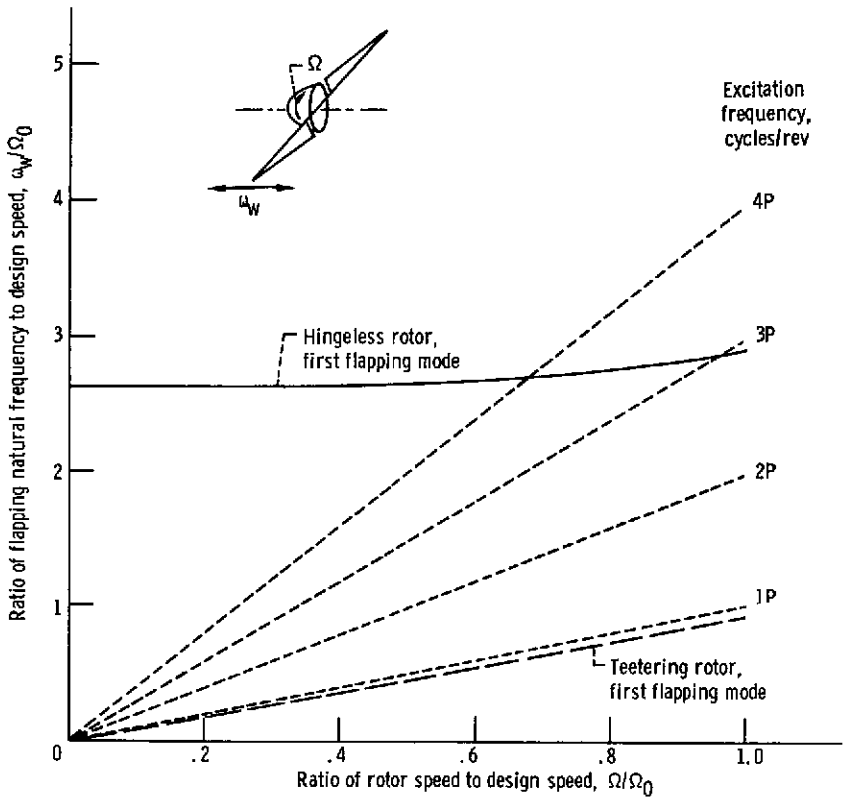

Figure 7. - Natural frequencies of hingeless and teetering blades. Design speed, Ω_0, 4.2 radians per second (40 rpm).

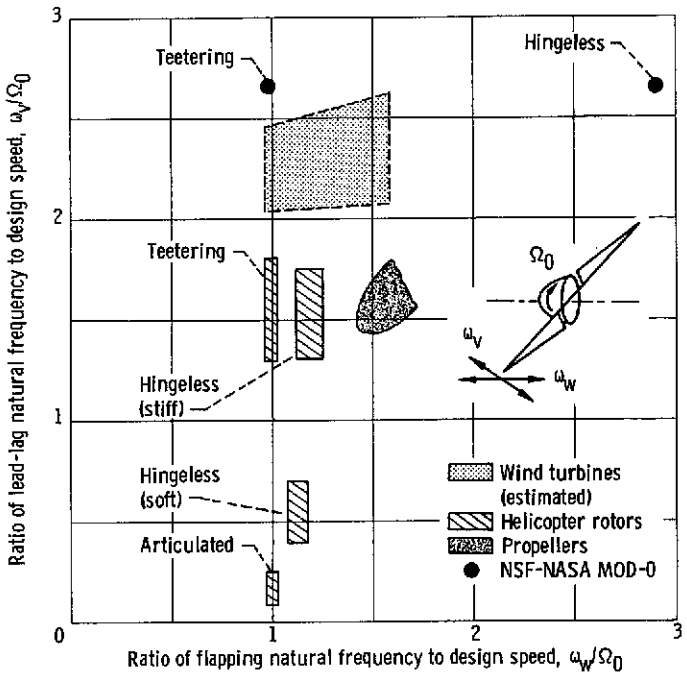

Figure 8. - Blade frequencies for various rotor systems. (Data from ref. 1, except NSF-NASA MOD-0.)

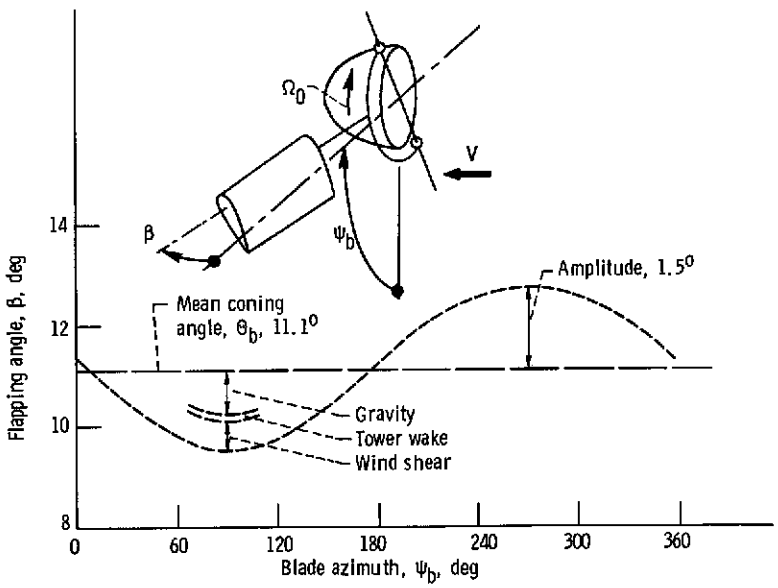

Figure 9. - Flapping motion of a hinged Mod-0 blade at rated wind speed of 8 meters per second (18 mph).

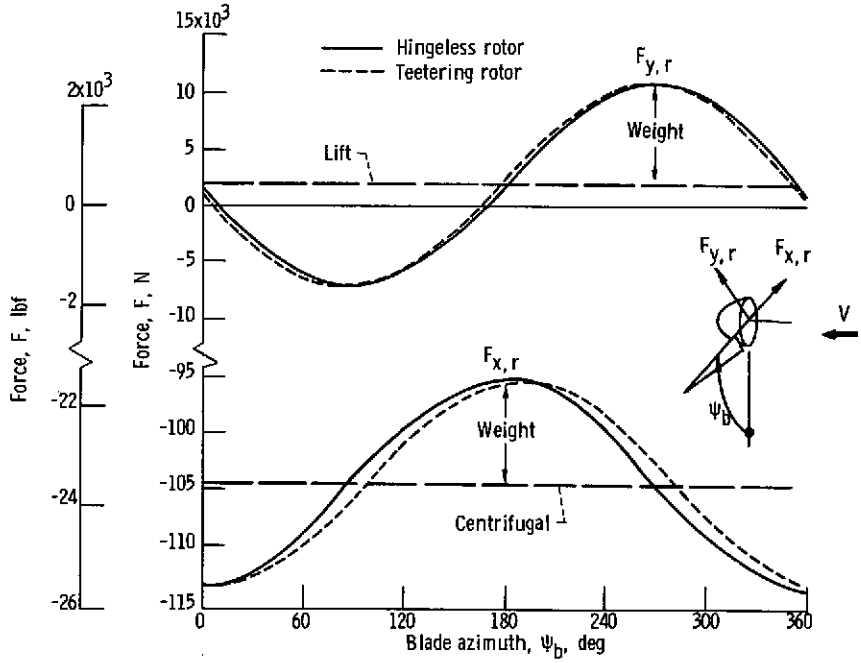

Figure 10. - Radial and tangential forces at a blade root at rated wind speed of 8 meters per second (18 mph).

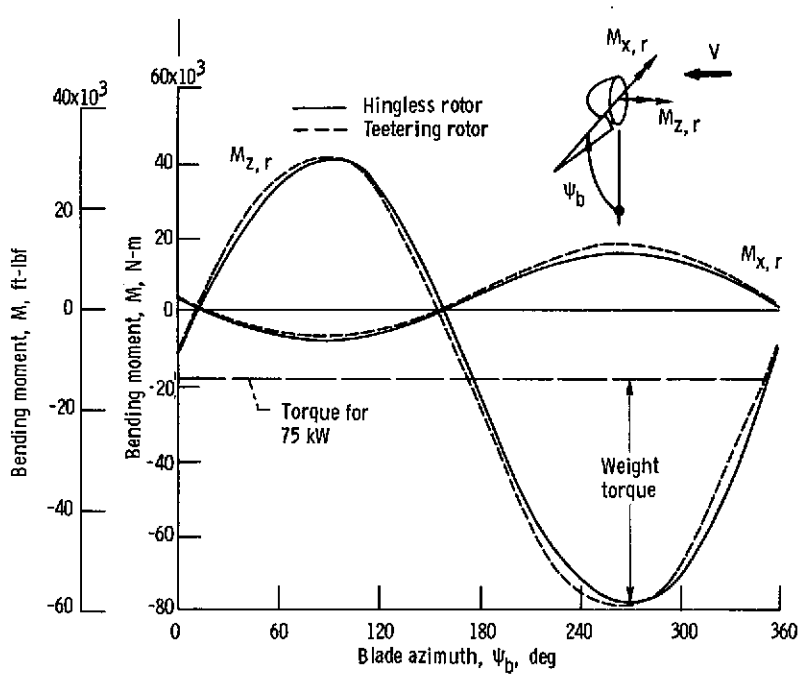

Figure 11. - Torque and twist moments at a blade root at rated wind speed of 8 meters per second (18 mph).

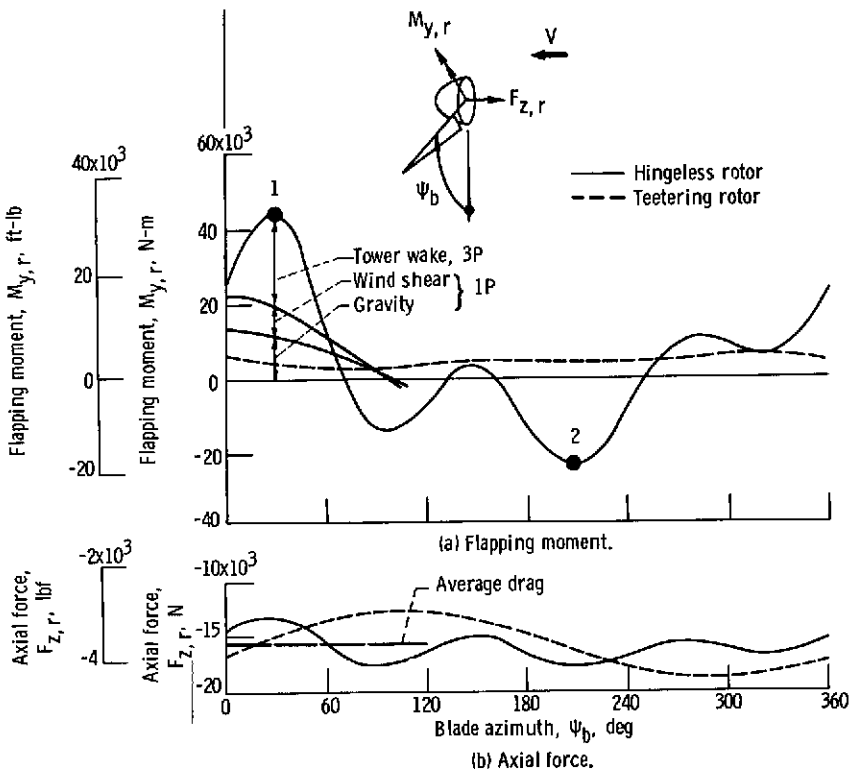

Figure 12. - Axial force and flapping moment at a blade root at rated wind speed of 8 meters per second (18 mph).

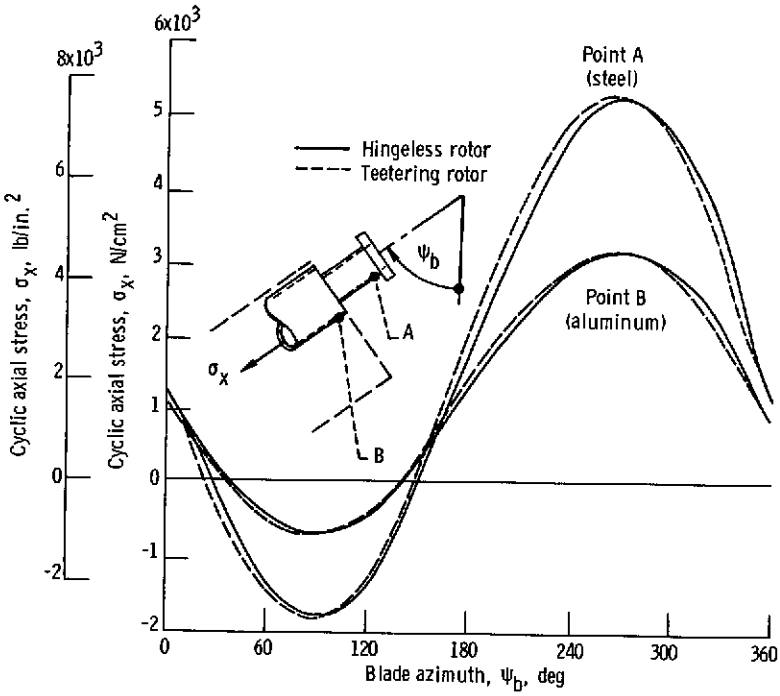

Figure 13. - Cyclic axial stresses in a blade shank at rated wind speed of 8 meters per second (18 mph).

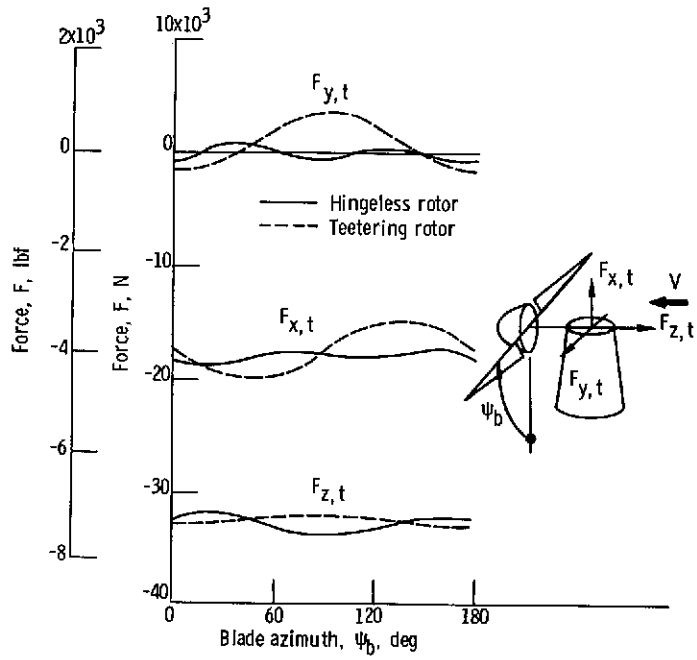

Figure 14. - Forces on tower from rotor at rated wind speed of 8 meters per second (18 mph).

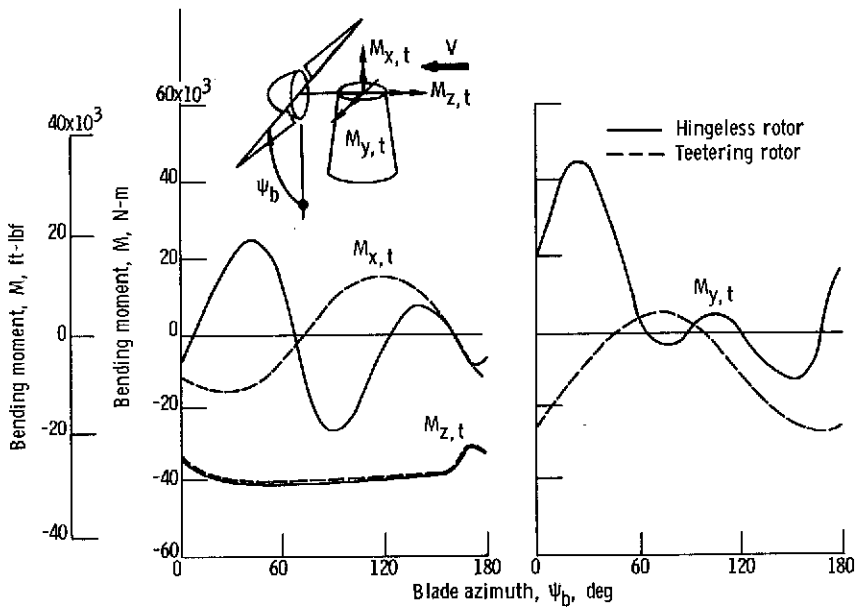

Figure 15. - Moments on tower from rotor at rated wind speed of 8 meters per second (18 mph).